Original

Tsimitri, C.; Rockel, B.; Wueest, A.; Budnev, N.M.; Sturm, M.; Schmid, M.:

Drivers of deep-water renewal events observed over 13 years in the South Basin of Lake Baikal.

In: Journal of Geophysical Research : Oceans. Vol. 120 (2015) 3, 1508 - 1526.

First published online by AGU: 12.03.2015

https://dx.doi.org/10.1002/2014JC010449

AGU PUBLICATIONS

JGR

Journal of Geophysical Research: Oceans

RESEARCH ARTICLE

10.1002/2014JC010449

Key Points:
- Mooring and wind data from Lake Baikal are analyzed to explain deep-water renewal
- Wind and seasonal stratification are important for deep-water volume replacements
- Three different types of deep-water renewal events were found in different seasons

Correspondence to:
C. Tsimitri,
chrysanthi.tsimitri@eawag.ch

Citation:
Tsimitri, C., B. Rockel, A. Wüest, N. M. Budnev, M. Sturm, and M. Schmid (2015), Drivers of deep-water renewal events observed over 13 years in the South Basin of Lake Baikal, *J. Geophys. Res. Oceans*, *120*, 1508–1526, doi:10.1002/2014JC010449.

Received 17 SEP 2014
Accepted 23 JAN 2015
Accepted article online 29 JAN 2015
Published online 12 MAR 2015
Corrected 18 MAR 2015

This article was corrected on 18 MAR 2015. See the end of the full text for details.

Drivers of deep-water renewal events observed over 13 years in the South Basin of Lake Baikal

Chrysanthi Tsimitri[1,2], Burkhardt Rockel[3], Alfred Wüest[1,4], Nikolay M. Budnev[5], Michael Sturm[6], and Martin Schmid[1]

[1]Eawag, Surface Waters—Research and Management, Kastanienbaum, Switzerland, [2]Institute of Biogeochemistry and Pollutant Dynamics, ETH Zurich, Zurich, Switzerland, [3]Institute of Coastal Research, Helmholtz–Zentrum Geesthacht, Geesthacht, Schleswig-Holstein, Germany, [4]Physics of Aquatic Systems Laboratory—Margaretha Kamprad Chair of Environmental Science and Limnology, ENAC, EPFL, Lausanne, Switzerland, [5]Applied Physics Institute, Irkutsk State University, Irkutsk, Russia, [6]Eawag, Surface Waters—Research and Management, Dübendorf, Switzerland

Abstract Lake Baikal, with a depth of 1637 m, is characterized by deep-water intrusions that bridge the near-surface layer to the hypolimnion. These episodic events transfer heat and oxygen over large vertical scales and maintain the permanent temperature stratified deep-water status of the lake. Here we evaluate a series of intrusion events that reached the bottom of the lake in terms of the stratification and the wind conditions under which they occurred and provide a new insight into the triggering mechanisms. We make use of long-term temperature and current meter data (2000–2013) recorded in the South Basin of the lake combined with wind data produced with a regional downscaling of the global NCEP-RA1 reanalysis product. A total of 13 events were observed during which near-surface cold water reached the bottom of the South Basin at 1350 m depth. We found that the triggering mechanism of the events is related to the time of the year that they take place. We categorized the events in three groups: (1) winter events, observed shortly before the complete ice cover of the lake that are triggered by Ekman coastal downwelling, (2) under-ice events, and (3) spring events, that show no correlation to the wind conditions and are possibly connected to the increased spring outflow of the Selenga River.

1. Introduction

Lake Baikal, the world's oldest, deepest and most voluminous lake is one of the most important aquatic biodiversity hotspots on the planet holding ~20% of the world's total freshwater. It is located in eastern Siberia covering an area of 31.7×10^3 km^2. Having been an isolated rift lake for ~25 million years it contains an intriguing sedimentary record for palaeoclimate reconstructions [*Mackay*, 2007] and it is home to hundreds of endemic species [*Moore et al*., 2009] populating the lake's entire water column of 1637 m maximum depth. The lake has been called the "Galapagos of Russia" due to its exceptional value to evolutionary science and in 1996 it has been awarded the World Heritage Site status by UN.

The water column below 250 m has a slight but permanent temperature gradient and it is largely isolated from the surface water dynamics and the atmospheric conditions. This gradient indicates a continuous downward flux of heat. However, even over many decades, no warming has been observed [*Shimaraev et al*., 1994], leading to the well-motivated hypothesis that a process is cooling the deep waters. As reported in the literature, episodic, advective-type, large-scale, deep-water intrusion events have been observed in the lake [*Hohmann et al*., 1997; *Schmid et al*., 2008; *Wüest et al*., 2005]. Proofs of the existence of such a mechanism are peaks of dissolved oxygen concentrations and observations of sudden temperature minima in the deepest layers of the lake [*Schmid et al*., 2008; *Weiss et al*., 1991]. These events bridge the hypolimnion and the near-surface layer by facilitating the transfer of heat over large spatial scales. They contribute to an effective turbulent mixing with vertical diffusivity values of the order of 1–10 cm^2 s^{-1} and turbulent eddies with vertical scales ranging from 10 to 100 m [*Lorke and Wüest*, 2002; *Ravens et al*., 2000]. While maintaining the permanent temperature stratification of the deep-water, these episodic intrusions contribute to the high hypolimnetic dissolved oxygen concentrations [*Weiss et al*., 1991] and facilitate the transfer of nutrient-rich water from great depths to intermediate and near-surface layers.

The deep-water renewal events have received considerable attention in the literature. Several studies have been made in order to calculate the deep-water renewal rates, the triggering mechanism, and the long-term effects on the heat budget, by employing different means as numerical modeling, chemical tracers, short-term mooring temperature data, and Conductivity-Temperature-Depth (CTD) casts (observations [*Hohmann et al*., 1997; *Shimaraev et al*., 1993; *Schmid et al*., 2008; *Weiss et al*., 1991; *Wüest et al*., 2005], and modeling [*Akitomo et al*., 1995; *Botte and Kay*, 2002; *Peeters et al*., 1997]).

Based on observational data, the proposed mechanisms that drive the deep-water renewal events are: spring thermal bars [*Shimaraev*, 1993], coastal downwelling [*Piccolroaz and Toffolon*, 2013; *Schmid et al*., 2008], and dense river plumes [*Hohmann et al*., 1997]. Most of these proposals were based on individual event studies rather than a collective overview. Here we propose a conceptual model of the driving mechanism of the deep-water renewal supported by long-term observational evidence. We provide a new insight into the triggering mechanisms by making use of: (1) continuous measurements over 13 years of moored thermistors and current meters at the neutrino site of the South Basin; (2) wind data calculated with a downscaled regional atmospheric model of the Lena catchment area of eastern Siberia provided by *Klehmet et al*. [2013]; (3) images from the MODIS satellite; and (4) several CTD casts recorded close to the thermistor monitoring location. Our postulate is that deep-water renewal in the lake is forced by the atmospheric conditions leading to coastal downwelling, which in turn leads to free convection depending on the thermal stratification of the near-surface waters.

We report a series of deep-water renewal events and describe and analyze the conditions under which they occurred. We categorize the events into winter, spring, and under-ice, according to season of observations and highlight the importance of the wind conditions, the stratification, and the bathymetric setting of the basin. The results suggest that: (1) the winter events are triggered by coastal downwelling when the Ekman transport increases abruptly, (2) the under-ice events are most probably triggered by similar mechanisms as the winter events before the complete ice coverage of the lake, and (3) the spring events are not driven by coastal downwelling and are possibly connected to the Selenga River discharge.

2. Site and Data

2.1. Site Description

Lake Baikal is located in southeast Siberia, between 51° and 56°N (Figure 1), an area with a strongly continental climate, with cold and dry winters leading to complete ice coverage of the lake for several months and short, warm summers [*Kouraev et al*., 2007]. It is located at an altitude of 456 m asl and is surrounded by high mountain ridges rising more than 2000 m. It has an elongated shape with a length of 636 km and a width varying between 25 and 80 km. It consists of three subbasins (South, Central, and North) separated by two high ridges that rise to depths of 260 m and 360 m below surface, respectively [*Delvaux et al*., 1997]. The three basins are extremely deep, with the Central Basin reaching a maximum depth of 1637 m, the South Basin 1461 m, and the North Basin 904 m [*De Batist et al*., 2002]. This specific bathymetry allows only for near-surface water exchange between the three basins and practically isolates the deep hypolimnia (Figure 1). A general cyclonic circulation is observed along the entire Lake Baikal coastline [*Troitskaya et al*., 2015], but each basin has its own cyclonic gyres as well [*Kouraev et al*., 2007]. The lake catchment is drained by more than 300, mostly minor, tributaries including three major rivers: Selenga, Upper Angara, and Barguzin. The Selenga delta located over the ridge that separates the South from the Central Basin is influencing locally the salinity and the nutrient budget in both basins. The lake's outlet, the Angara River, is located at the South Basin, with an average discharge of 65.3 $km^3\ yr^{-1}$ [*Sapota et al*., 2006].

2.2. Mooring Data and Calibration

A monitoring station with moored thermistors and current meters has been installed in March 2000 at the north shore of the South Basin (Figure 1) as part of a joint research project by the Applied Physics Institute of Irkutsk State University and the department "Surface Waters—Research and Management" of Eawag, Switzerland. At present, three mooring lines are deployed: mooring Long, L, since March 2000, mooring Hydra, H, and mooring Shore, S, both since March 2004. They are placed in a triangle shape with moorings L and H 1 km apart, reaching a depth of 1350 m at a distance of 3.6 km from the northern coast, and mooring S reaching a depth of 547 m, deployed 1.2 km from the coast (Figure 1). Occasional CTD casts, taken

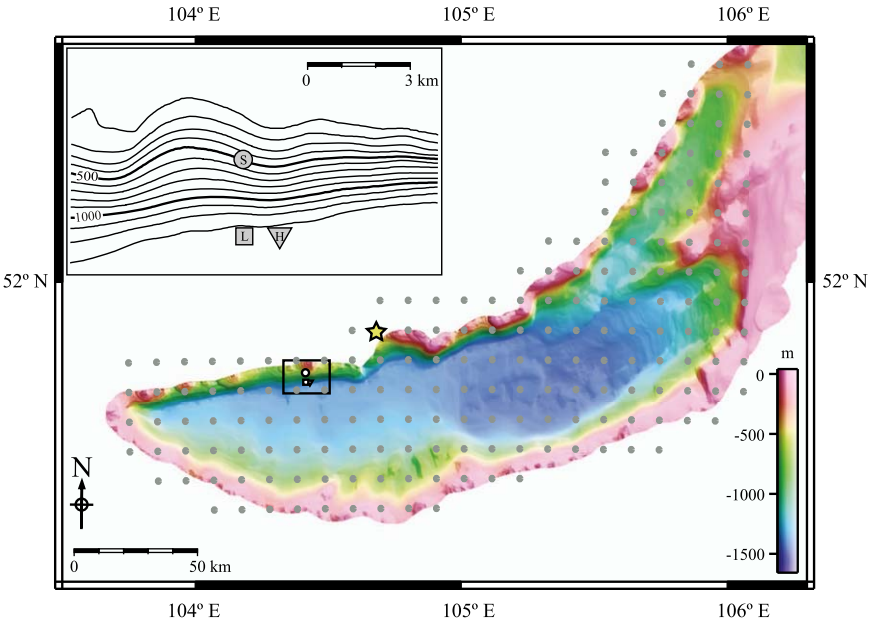

Figure 1. Bathymetric map of the South Basin of Lake Baikal based on data of *De Batist et al.* [2002]. The gray dots indicate the wind model grid points (grid width 7 km). The maximum depth of the basin is 1461 m. A ridge rising up to 260 m below surface separates this basin from the Central Basin. Three moorings were deployed at the northern shore of the South Basin: L (depth: 1350 m), H (depth: 1350 m), and S (depth: 547 m). The closest meteorological station to the monitoring area is close to Listvyanka denoted with a star.

with a Sea-Bird SBE 25 Sealogger close to the monitoring area, were provided by the Limnological Institute of the Siberian Branch of the Russian Academy of Science (Irkutsk) for calibration purposes.

The three moorings are equipped with different types of thermistor loggers recording in-situ temperature at regular intervals varying between 15 s and 60 min. The logger types used are: Vemco 12 bit minilog 64K (resolution 0.015°C, accuracy 0.1°C), RBR TR-1000 (resolution 0.002°C, accuracy 0.05°C), TR-1050 (resolution 0.0001°C, accuracy 0.002°C), TR-1060 (resolution $<$ 0.00005°C, accuracy 0.002°C), and TDR-2050 (resolution 0.0001°C, accuracy 0.002°C). Two Aanderaa RMC7 current meters measuring current speed and direction (resolution 0.007 m s^{-1}, accuracy 0.01 m s^{-1}, threshold 0.02 m s^{-1}) have been interchangeably placed between moorings L and S. The thermistors were recovered annually in March for maintenance and for downloading the data. They were redeployed within 1–2 days. The configuration of the thermistors on the mooring strings varied each year depending on the monitoring adjustments.

The accuracy of the thermistors was tested and confirmed in the laboratory. Most of the sensors were calibrated using an automated temperature stepping program (Hart Scientific 7025 High Precision Bath) once or twice during the sampling period, and the data were corrected to the nearest calibration date. The Vemco thermistors were restrictively deployed only at shallow depths where a high-resolution or accuracy is not needed.

To assure the coherence of the sensor measurements, we performed additional on-site calibrations with two different methods. Starting in March 2010 and each year thereafter, the loggers of each mooring were bundled together and submerged for several hours below 200 m, where the temperature variations for the submersion period do not exceed 0.001°C. A reference thermistor logger was chosen and the rest were adjusted accordingly. For the years preceding 2010, a CTD cast calibration was done: the thermistor data were coupled to the CTD measurement taken at the proximity of mooring L. With this method, we were able to calibrate only mooring L for depths deeper than 250 m where the temperature gradients are weak. The recordings were corrected only when the temperature difference to the CTD measurement was larger than the accuracy of the logger. Moreover, in order to facilitate the analysis, we resampled the data on a regular time grid (not all the thermistors on each mooring line are sampling at equal intervals). In this study, we are not interested in the short-term temperature variations so we defined the time grid for each year and mooring according to the longest sampling interval (20 min for most years).

2.3. Wind Data

The closest meteorological station to the mooring area providing consistent measurements is located in Listvyanka, approximately 30 km northeast of the mooring site (Figure 1). Due to the topography, the wind field is highly variable in the region. The on-shore measurements must be expected to be far from representative for the wind over the lake, thus making the data from the meteorological station not suitable for assessing the relationships between the wind and in-lake physical processes. An alternative is to use wind data from atmospheric reanalysis, ideally at high regional resolution. However, for the Lake Baikal area only global reanalysis data are available. The grid mesh of about 200 km for NCEP-RA1 [*Kalnay et al*., 1996] and 90 km for ERA-Interim [*Dee et al*., 2011] global reanalysis are too coarse to resolve the local wind features over the lake. Furthermore the lake is either missed totally (NCEP-RA1) or partly (Southern Basin in ERA-Interim) by these data. A solution for this problem is a dynamic downscaling of the reanalysis data by a high-resolution regional atmospheric model.

In our study, we used version 4.8 of the COSMO-CLM or short CCLM (COSMO model in climate mode, *Rockel et al*. [2008]) based on the formerly named "Lokalmodell" [*Steppeler et al*., 2003]. The CCLM is a nonhydrostatic regional atmospheric model and shares the same source code with the weather forecast model of the German Weather Service. It is based on the thermohydrodynamic equations describing the compressible flow in the atmosphere.

Klehmet et al. [2013] performed a regional downscaling of the global NCEP-RA1 reanalysis product over large parts of Siberia including the Lake Baikal area with a horizontal grid width of 50 km. However, even with this resolution, the local features of Lake Baikal cannot be captured and the Southern Basin is missing. Wind velocities are still too low (very rare events with wind speeds > 10 m s^{-1}) and the wind direction is still equally distributed with a tendency to winds perpendicular to the lake. Therefore, a further nesting of the model down to a grid width of 7 km was necessary for this study. With this, the wind flow can be described and wind speeds > 10 m s^{-1} occur more often. However, because the wind data are hourly instantaneous values, short high-wind peaks cannot be captured. Even though this results in an underrepresentation of the high-wind speeds when comparing with the observations at Listvyanka, we decided to use the model output as it represents the general wind trends.

2.4. Satellite Data

To determine the period of ice cover, we used satellite images from the Moderate Resolution Imaging Spectroradiometer (MODIS) sensor onboard the EOS-AM-1 (TERRA) satellite (channels 1 and 2), with a spatial resolution of 250 m. By visual inspection, we determined the first and the last day of ice cover at the monitoring site.

3. Physical Characteristics and Methods

In Lake Baikal, the dissolved ions and particulate matter concentrations are low and almost constant with depth contributing little to the density stratification [*Ravens et al*., 2000]. Temperature is the main parameter defining the stratification throughout the water column with a few exceptions, like the region where the thermal expansivity of water is equal to zero and possibly regions close to river mouths, where inflows can have a greater salinity and a higher particle concentration than the lake. The potential temperature, $\theta = T - \int \Gamma dz$, is almost equal to the in situ temperature T, as the adiabatic lapse rate, Γ, is extremely low, and the difference between T and θ is a few 0.0001°C [*Wüest et al*., 2005].

The water column of the South Basin can be separated in three zones in terms of temperature and stratification. The surface layer (top 250 m) follows a seasonal variation and mixes twice per year in December and in June, before and after the ice cover (Figure 2). The exact depth of the seasonal mixing varies from year to year between 150 and 250 m. From approximately mid-January to the beginning of May, the surface is ice covered and the temperature increases with depth reaching 3.6°C at 150 m. In these months, the squared Brunt-Väisälä frequency (N^2) is more than 10^{-6} s^{-2} restricting vertical exchange (Figure 2). When the ice breaks, the surface warms up and gradually increases to a maximum of ~18°C in late summer. During the transition between inverse winter stratification and summer stratification, the surface layer is convectively mixed at a temperature of 3.6°C, and N^2 decreases to values smaller than 10^{-7} s^{-2}. At the end of September, the layer gradually cools down to reach 0°C at the surface in January. The convectively mixed state is observed again in mid-December just before the ice cover forms. These two seasonal mixing periods provide the windows in time when deep-water renewal events can be initiated; the process will be described

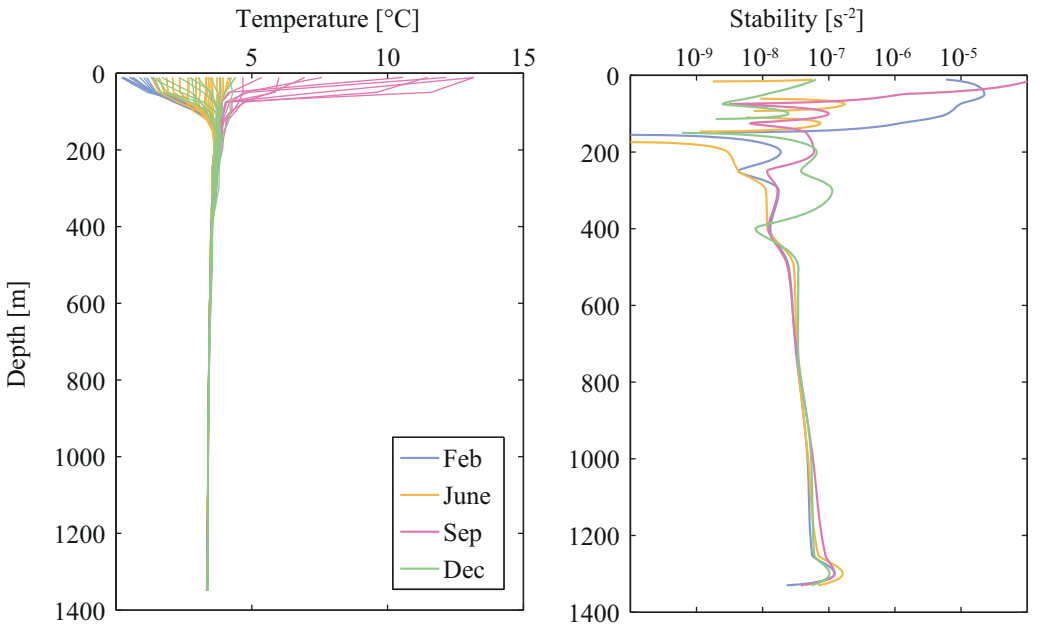

Figure 2. (left) Annual variation of the temperature profile in the South Basin of Lake Baikal. The four colors reflect the seasonal changes of the surface layer (0–250 m). Blue lines: 15 January to 15 May (ice covered period); orange lines: 15 May to 30 June (spring mixing period); purple lines: 1 July to 30 November (summer and autumn stratified period); green lines: 1 December to 15 January (late autumn mixing period). Below 250 m, the temperature is approximately constant throughout the year. (right) The squared Brunt-Väisälä frequency, N^2, calculated for one representative profile of each season. The data used to produce the figures are from the monitoring year 2005/2006 at mooring L.

in detail later. Below this seasonally stratified layer follows the intermediate, permanently stratified deep-water layer (PSDW) that covers most of the depth, down to 1250 m. In this layer, the temperature and consequently the stratification are constant within 0.3°C throughout the year. The temperature gradient is 0.02°C per 100 m, establishing an extremely low N^2 $O(10^{-8}\ s^{-2})$ and thus facilitating mixing. Last the bottom layer below 1250 m is characterized by episodic cooling events that can lead to sudden deviations from the background temperature of 3.35°C by a few tenths or hundredths of a degree Celsius.

The wind over Lake Baikal is highly influenced by the surrounding steep mountains. It tends to blow parallel to the coast either northeasterly or southwesterly. Statistically, the strongest winds are observed in January and February when the lake is ice covered, blowing from the northeast. Winds in the opposite direction are also prevalent and can be quite strong around the year. Southeasterlies are rarely observed throughout the year. A monthly climatology of the wind conditions from 2000 to 2013 at the monitoring area is depicted in Figure 3 with wind roses indicating direction, intensity, and frequency of occurrence.

3.1. Temperature of Maximum Density

Crucial for the deep-water renewal in Lake Baikal is the pressure-dependence of the temperature of maximum density, T_{md}, of water. At atmospheric pressure, fresh water has its maximum density at ~3.984°C. If a water parcel with temperature higher than T_{md} warms up it becomes lighter while if the initial temperature of the parcel was lower than T_{md} a warming will result in denser and thus heavier water. As pressure increases with depth, the structure of the water molecule clustering changes, giving rise to a higher density at all temperatures, with especially pronounced effects at lower temperatures [*Cotter*, 2010]. In freshwater T_{md} decreases with depth according to the relationship:

$$T_{md} = 3.984^{\circ}C + 0.0021z \quad (1)$$

where z(m) is the vertical coordinate (positive upward). For example at a depth of 600 m, T_{md} is 2.726°C. This reduction of T_{md} with depth is the key mechanism for deep-water renewal in Lake Baikal as it leads to a special type of convective instability, the so-called thermobaric instability [*Shimaraev et al.*, 1993], that facilitates the sinking of water masses when the temperature stratification allows for it.

The alteration of the water clustering under pressure allows for a water parcel to change its in situ density, ρ, without changing its temperature, by an adiabatic displacement to a new depth. If the new in situ density

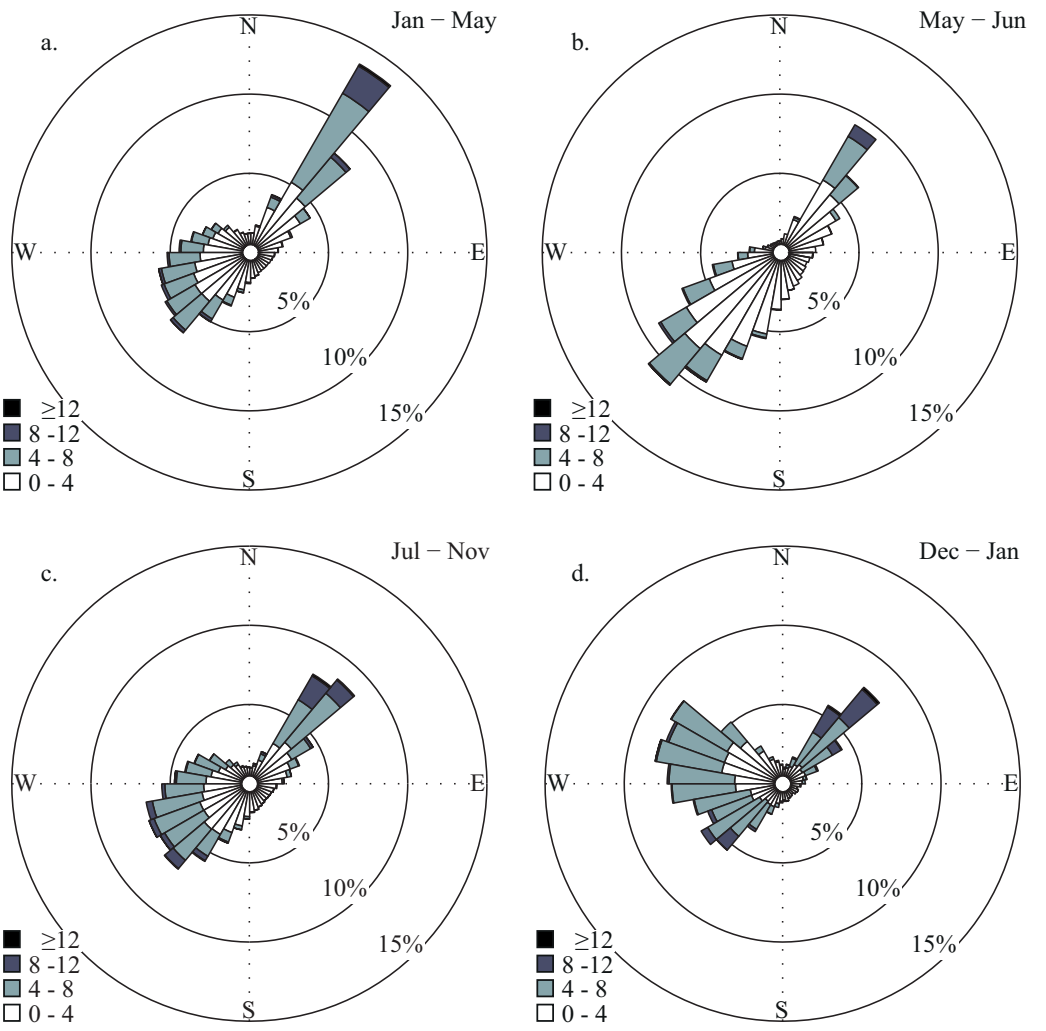

Figure 3. A seasonal climatology of the wind conditions at the monitoring area produced by the regional downscaling of the global NCEP-RA1 reanalysis product. The seasonal wind roses indicate direction and intensity of the wind in m s^{-1}. The four seasonal periods are defined in Figure 2 and in the text.

of the parcel is larger than that of the ambient water at the final depth, it will sink further until it will be neutrally buoyant. At constant pressure (depth), density depends solely on temperature and the difference of the temperature to the T_{md} is a simple indicator of whether a parcel will sink or not at the new depth. One can consider a near-surface water parcel (Figure 4) with a temperature of 3.3°C ($\rho = 1.00009845$ kg m^{-3} at 10 m) being adiabatically displaced to a 250 m depth where the ambient temperature is 3.7°C and $\rho = 1.00126435$ kg m^{-3}. At this depth, the surface parcel's temperature is closer to the local T_{md} (3.459°C) and thus the parcel is denser, $\rho = 1.00126473$ kg m^{-3}, than the ambient water, resulting in a further sinking to greater depths (Figure 4). This mechanism, proposed by *Weiss et al.* [1991] for renewing the deep-water of Lake Baikal, was observed and thoroughly analyzed by *Schmid et al.* [2008]. This mechanism is possible in Lake Baikal prior and after the ice cover, when the near-surface temperature is equal or lower than the bottom layer temperature of 3.35°C.

3.2. Thermobaric Instability Drivers

For thermobaric instability to take place, a triggering mechanism has to initially displace the near-surface water. *Schmid et al.* [2008] studied in detail one of the most prominent deep-water renewal events observed in the South Basin, and showed that thermobaric instability was initiated by coastal downwelling at the north coast of the South Basin. They used temperature data from mooring S and mooring L to trace the path of the downwelled water mass from the surface layer close to the shore to the local bottom of the

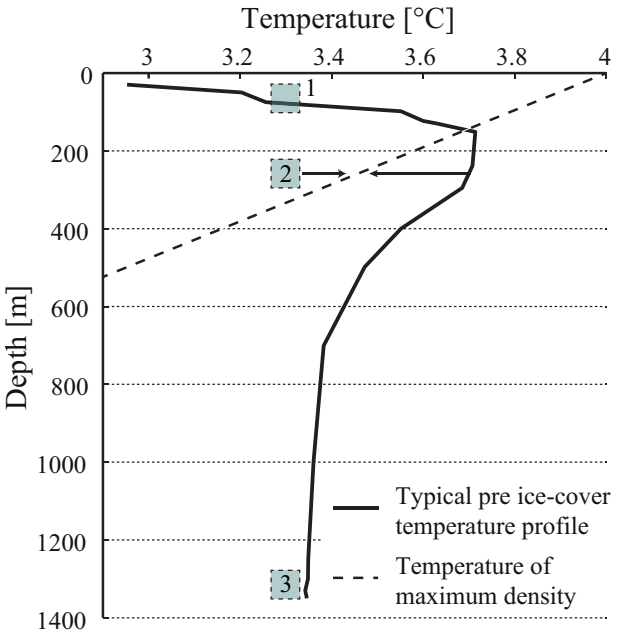

Figure 4. Mechanism of thermobaric instability for a typical winter temperature profile (solid line) and vertical profile of the temperature of maximum density (dashed line): the density of a near-surface colder water mass (1) changes when it is forced downward. If at the new depth (2), the downwelled water mass is denser than the ambient water, it will sink freely to the local bottom of the lake or to the depth of equilibrium density (3).

basin at 1350 m. By using a large number of CTD casts for a period of 2 years (1993–1995), *Hohmann et al*. [1997] studied the deep-water mechanisms in all basins and their conclusions were sound mainly for the Central Basin, where they identified the springtime saline and cold water outflow of the Selenga River as the main trigger. While they did not exclude the possibility of wind triggering, they did not have appropriate observations to discuss it further. *Schmid et al*. [2008] proposed that all of the deep-water renewal events observed in the South Basin data set were triggered by coastal downwelling.

To investigate this hypothesis, we formulate the following conceptual model: (1) Surface water is transported towards the north coast by Ekman transport triggered by strong NE winds. (2) When the gravitational force of the water piling up exceeds the horizontal pressure gradient force, the isotherms are depressed. (3) If the surface layer is convectively mixed, the buoyancy force is low and the isotherm depression can reach the critical depth where the thermobaric instability is initiated. (4) The sinking water mass will slide down the steep northern slope and will reach the bottom of the basin given that the temperature of the sinking water is lower than the bottom temperature; if not the sinking water will intrude at some intermediate level of equilibrium density in the PSDW layer [*Piccolroaz and Toffolon*, 2013]. This sequence of steps is tested on the 13 years data set of temperature, lake water currents, and wind from the reanalysis model.

3.3. Ekman Transport

To estimate the coastal Ekman transport, we first calculate the wind stress at each grid point of the reanalysis model over the lake. The wind stress is given by:

$$\begin{cases} \vec{\tau}_x = \rho_a C_{10} |U| \vec{u} \\ \vec{\tau}_y = \rho_a C_{10} |U| \vec{v} \end{cases} \tag{2}$$

where x is the west-east axis, y the south-north axis, $\vec{u}$ and $\vec{v}$ are the wind components in the x and y directions, respectively, and U is the wind speed at 10 m. $\rho \approx 1.34$ kg m^{-3} is the air density at -10°C. The drag coefficient at 10 m, C_{10}, depends on the wind speed and the wave development state [*Wüest and Lorke*, 2003]. The size of Lake Baikal allows for a wind fetch large enough to produce waves not far from being fully developed (full development for $U = 6$ m s^{-1} requires ~100 km fetch). For $U > 5$ m s^{-1}, C_{10} can be approximated with the following equation: $C_{10} \approx \left[k^{-1} \ln\left(g10/C_{10}U_{10}^2 + K\right)\right]^{-2}$ [*Wüest and Lorke*, 2003], converging after four iterations, with $k = 0.41$ the von Karman constant, $g = 9.81$ m s^{-2}, $K = 11.3$ a nondimensional constant determined by *Smith* [1988] and *Yelland and Taylor* [1996], and 10 has the units of meter.

We introduce the new grid point specific coordinate (p, q), rotated anticlockwise by a variable angle φ with respect to the (x, y) system, such that the q direction is always normal to the coastline at each grid point and p is parallel to the coast. The new wind stress is:

$$\begin{cases} \vec{\tau}_p = \cos\phi \ \vec{\tau}_x - \sin\phi \ \vec{\tau}_y \\ \vec{\tau}_q = \sin\phi \ \vec{\tau}_x - \cos\phi \ \vec{\tau}_y \end{cases} \tag{3}$$

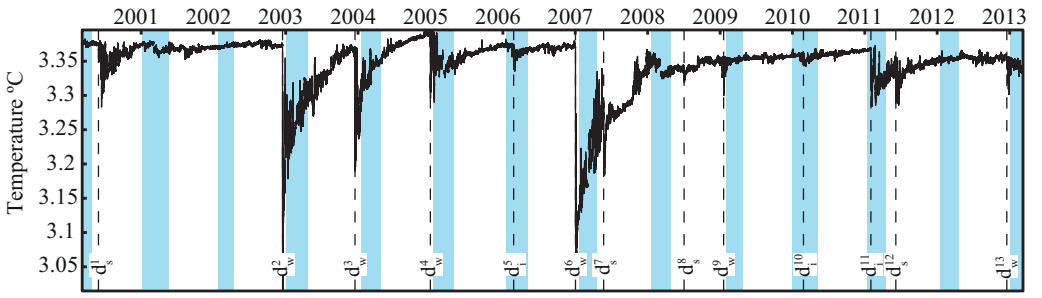

Figure 5. Variation of the bottom temperature in 1350 m depth at the monitoring site of the South Basin (mooring L). The vertical-dashed lines indicate the dates when the minimum temperature of each event was observed. The blue bands indicate the ice covered periods at the monitoring site. The indices stand for the seasonal periods: ice (i), spring (s), and winter (w).

In this coordinate system, the Ekman transport towards the northern coast, $\vec{M}_q$, is directly proportional to the wind stress in the p direction.

$$\begin{cases} \vec{M}_p = \dfrac{\vec{\tau}_q}{f\rho_E} \\ \vec{M}_q = \dfrac{\vec{\tau}_p}{f\rho_E} \end{cases} \tag{4}$$

where ρ_E is the in situ average density of the Ekman layer and f (0.0001137 s^{-1}) the local inertial frequency.

4. Observations

4.1. Decadal Variations of the Bottom Layer Temperature

The temperature below 250 m depth does not show any seasonal variations but in the bottom layer ($>$ 1250 m depth) we occasionally observed sudden and considerable temperature decreases of up to a few 0.1°C. A total of 13 such disturbances have been recorded (Figure 5 and Table 1). We refer to these cold water intrusions that reach the bottom of the South Basin as events and we label them in a consecutive manner with the superscript indicating the order of occurrence and the subscript (w for winter, i for under-ice, and s for spring) for the season of appearance (d_s^1, d_w^2, . . .). From now on, we will use the term "bottom of the lake" to refer to the deepest water volume of the South Basin. The decrease of the temperature is between 0.02 and 0.1°C, with two exceptionally cold events in the winters of 2002/2003 and 2006/2007 where the temperature dropped by more than 0.3°C (Figure 5).

Table 1. Properties of Bottom-Reaching Cold Intrusion Events Observed in the South Basin of Lake Baikal from 2000 to 2013[a]

Event	Date of Observed T_{down}	Season	T_{down} (°C)	ΔT (°C)	Current Speed 16 m Depth (m s^{-1})	Current Speed 1350 m Depth (m s^{-1})	Intrusion Volume (km^3)
d_s^1	16 Jun 2000	Spring	3.283	−0.075	-	-	43
d_w^2	17 Dec 2002	Winter	3.015	−0.375	-	-	171
d_w^3	17 Dec 2003	Winter	3.190	−0.14	-	-	111
d_w^4	19 Jan 2005	Winter	3.291	−0.095	0.12	-	59
d_i^5	1 Mar 2006	Ice	3.336	−0.033	n/c	-	69
d_w^6	5 Jan 2007	Winter	3.057	−0.316	0.16	-	203
d_s^7	28 May 2007	Spring	3.184	−0.102	0.07	0.07	165
d_s^8	3 Jul 2008	Spring	3.322	−0.024	n/c	n/c	44
d_w^9	19 Jan 2009	Winter	3.301	−0.052	0.02	0.05	19
d_i^{10}	25 Feb 2010	Ice	3.343	−0.016	*	n/c	76
d_i^{11}	5 Feb 2011	Ice	3.284	−0.084	0.07	0.04	62
d_s^{12}	20 Jun 2011	Spring	3.286	−0.065	0.09	0.04	27
d_w^{13}	28 Dec 2012	Winter	3.301	−0.042	*	0.06	28

[a]The day and the season of observation, the minimum temperature for each event (T_{down}), and the difference to the background temperature (ΔT), the mean surface current speed (10 days before until the date of observed T_{doown}) and the bottom current speed (6 days before until 10 days after the observed T_{down}) (whenever available), and the estimated intruding volume. (*) indicates current meter failure, n/c: no current.

Most of the events (six) occurred in wintertime, just before ice cover, in December and January, including the two coldest ones d_w^3 and d_w^6. Three very weak events were observed when the lake was ice covered in February and March and four in spring, immediately following the ice breakup. After each event, the temperature recovered approximately exponentially to the background value within a few months and in some cases in an adjustment time scale of almost 1 year.

To investigate the driving mechanism of the observed events, it is necessary to use the mooring deployed closer to the shore (S). We focus on the events taking place after 2004, the year that mooring S was installed. For each event, we plot the isotherm displacements as observed in moorings S and L, a few days before and after the minimum temperature was recorded at the bottom of the basin (Figure 6).

If an event is the consequence of coastal downwelling taking place at the monitoring site, we should observe the isotherms at the shore being depressed to a level that free convection is initiated and surface water can be transported to greater depths sliding down the shelf. The above process is clearly the case for three of the recorded events, d_w^6, d_w^9, d_w^{13} (Figure 6) and it is most probably the case for the event d_w^4. In the latter event, we can assume that the isotherm depression did not take place exactly at the monitoring location but close nearby. Thus, our temperature measurements are not close to the midpoint of the convecting water masses and we are most probably observing the process from a peripheral location. All the above four events occurred in the wintertime. The shore isotherms were not depressed for the rest of the events (Figure 6). Two questions arise from these observations: (1) Do the events that follow the shore isotherm depression share some common characteristics? (2) What is the driver, if not downwelling, for the rest of the deep intrusion events?

According to *Schmid et al*. [2008] who analyzed in detail the event d_w^6, taking place in January 2007, strong downwelling favorable winds (easterlies) were present over the South Basin for a period of 6 days before the temperature dropped at the bottom of the lake. A westward alongshore surface current was recorded by the current meter placed at 16 m depth with a small cross-shore component that led to the depression of the isotherms close to the shore. Approximately after 50 h, a cold water mass appeared at the bottom of the lake at moorings L and H. Based on the different arrival times of the cold front between the two moorings, *Schmid et al*. [2008] estimated an eastward bottom current with a speed of 0.012 m s^{-1}. However, this estimate was false due to an error in the time allocation for one of the moorings, and recalculation showed that the real flow direction was westward (anticlockwise). In the following, we examine the wind field and current measurements, whenever available, and look for common characteristics and similar patterns for the different deep intrusion events.

4.2. Wind Variability

The wind field over the monitoring site for a period of 20 days before the events is shown in Figure 6 for events following d_w^4. The wind is predominately blowing from northeast (35°) with high speeds ($>$ 8 m s^{-1}) regularly recorded before events d_w^3, d_w^4, d_i^5, d_w^6, d_s^7, d_w^9 (Figure 6, event d_w^3 not shown). These are the ideal conditions for downwelling to be initiated. The wind pattern for the rest of the events (d_s^1, d_w^2, d_s^8, d_i^{11}, d_s^{12} and d_w^{13}) is not associated with downwelling.

4.3. Currents

Two mechanical current meters were mounted on the mooring lines in March 2004. One has been located at 16 m depth at mooring S since then and the other, originally placed at 547 m at mooring S, was moved to the bottom of mooring L at 1350 m in 2007. In 2009 and in 2012, the upper current meter did not function between November and March of the following year. We thus have no information for the surface currents for events d_s^1, d_w^2, d_w^3, d_i^{10}, and d_w^{13}. For the remaining eight events, we calculate the mean speed for a period of 15 days prior to each event, where all measurements below the threshold (0.02 m s^{-1}) were replaced with half of the threshold value (0.01 m s^{-1}). Significant near-surface current activity was recorded before the winter events d_w^4 and d_w^6 (mean speed of 0.11 and 0.14 m s^{-1} and maximum speed of 0.36 and 0.43 m s^{-1}, respectively). Before the spring events, d_s^7 and d_s^{12} surface currents were observed but they were not strong (mean speed of 0.05 and 0.07 m s^{-1} and maximum speed of 0.18 and 0.26 m s^{-1}, respectively). Before the under-ice event d_i^5 taking place a long time after ice cover (first sign of downwelling observed 40 days after complete ice cover), no currents were observed as expected. However, currents were observed 2 days after complete ice cover in January 2011, eleven days before event d_i^{11}. No surface

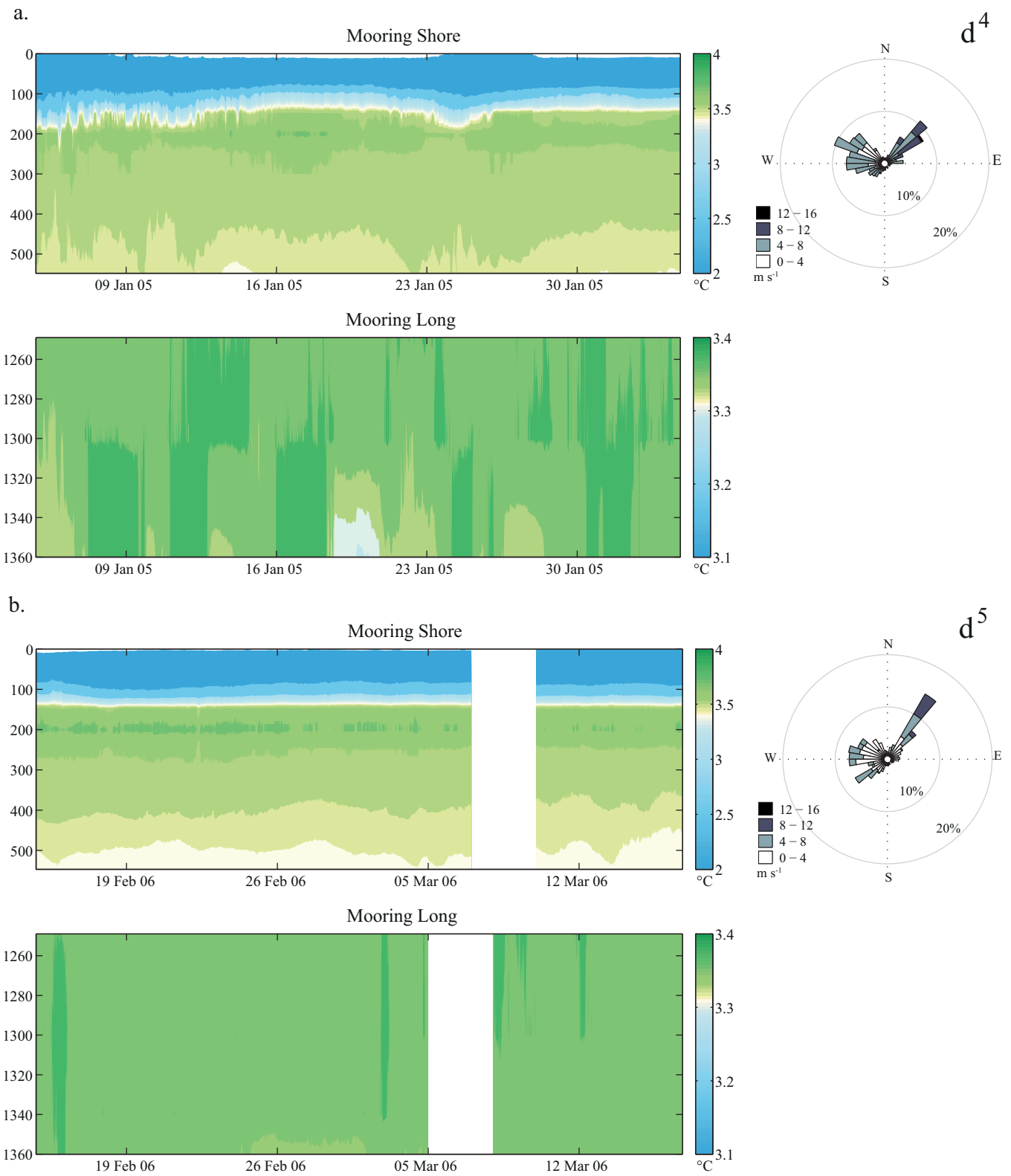

Figure 6. Observations of the events $d_w^4 - d_w^{13}$, subfigures (a)–(j). (left) Isotherm contours (in °C) around the period of the event at mooring S (0–550 m; top) and at mooring L (only below 1250 m; bottom), the depth y axis is in meters. (right: top) Prevalent wind over the monitoring site for a period of 20 days before each event, direction shows where the wind is blowing from (numbers are in m s^{-1}). (right: bottom) Current meter measurements at 1350 m at mooring L for the events following d_s^7 (d). Currents are shown for a period of 6 days before until 10 days after the event and direction indicates where the current is going to. The frequencies of occurrence do not add up to 100% because often the currents are below the threshold of 0.02 m s^{-1}.

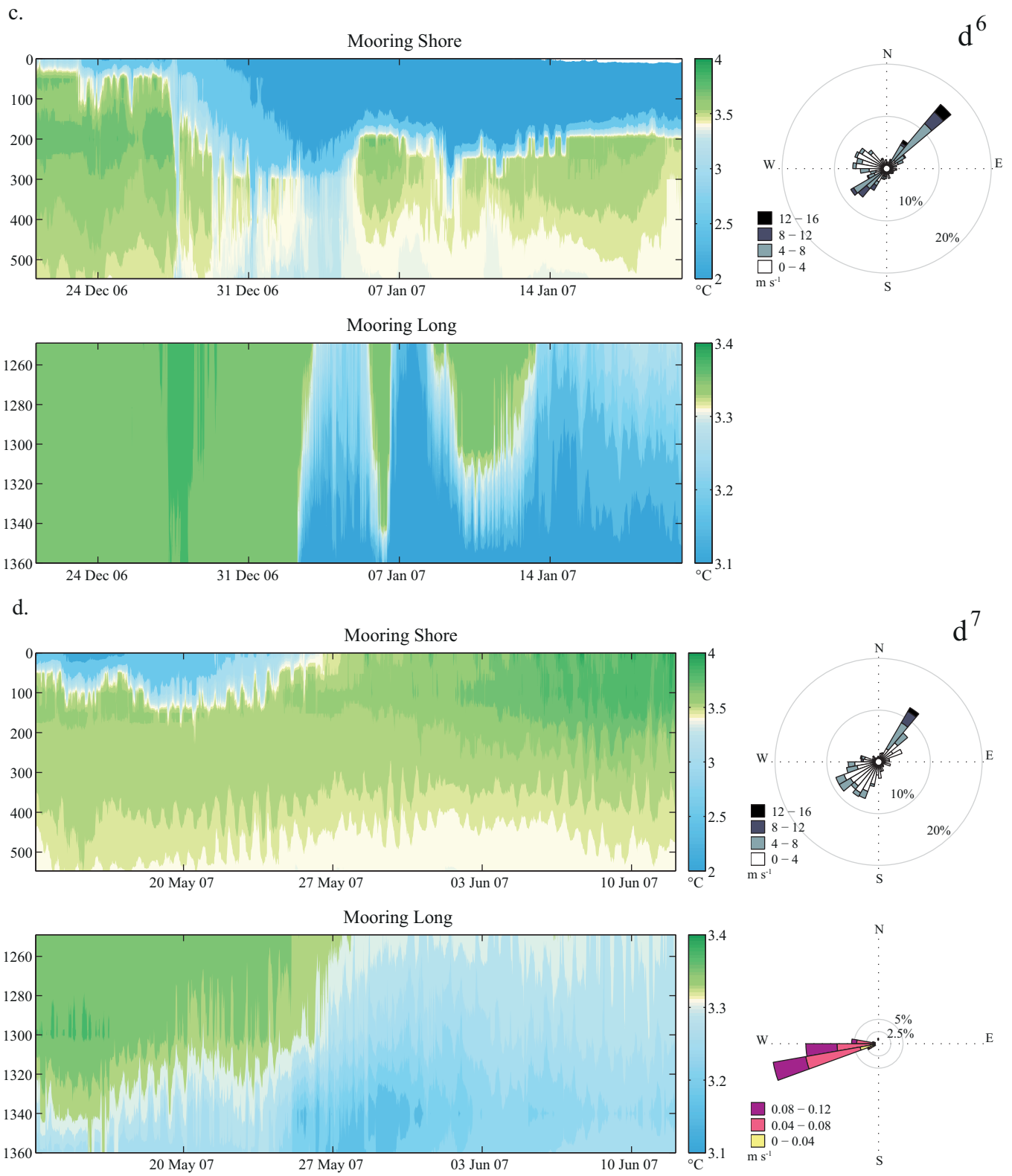

Figure 6. (continued)

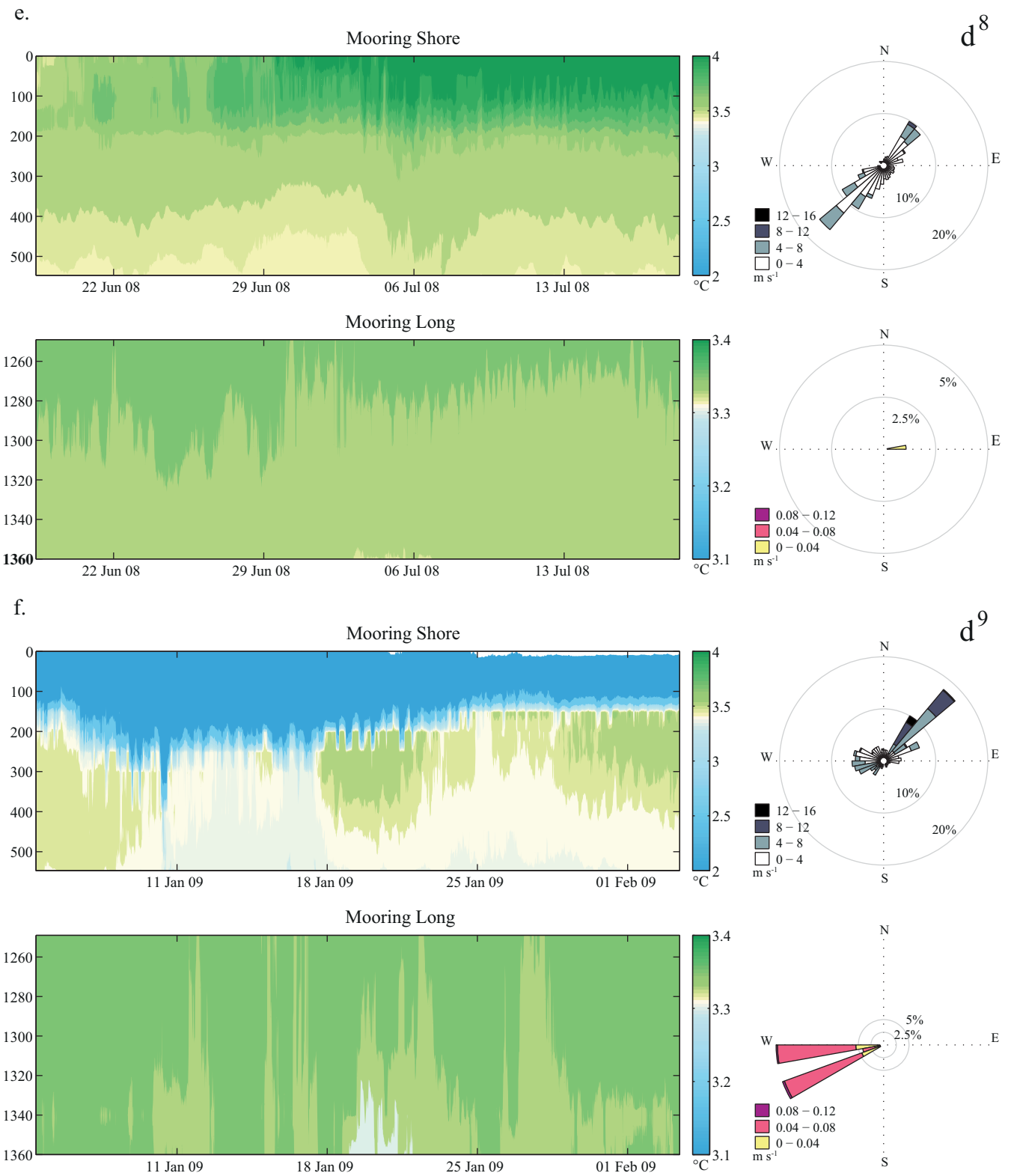

Figure 6. (continued)

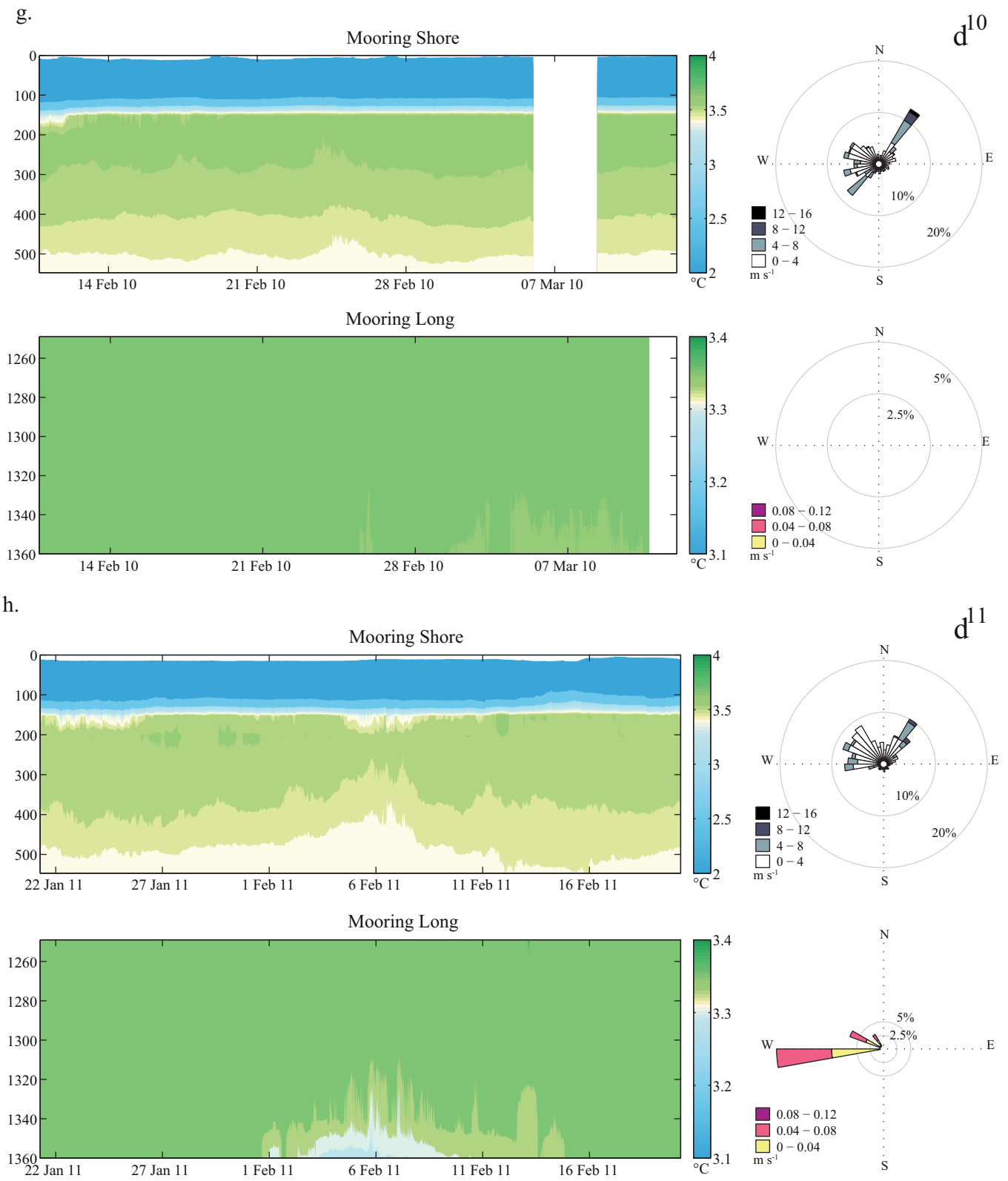

Figure 6. (continued)

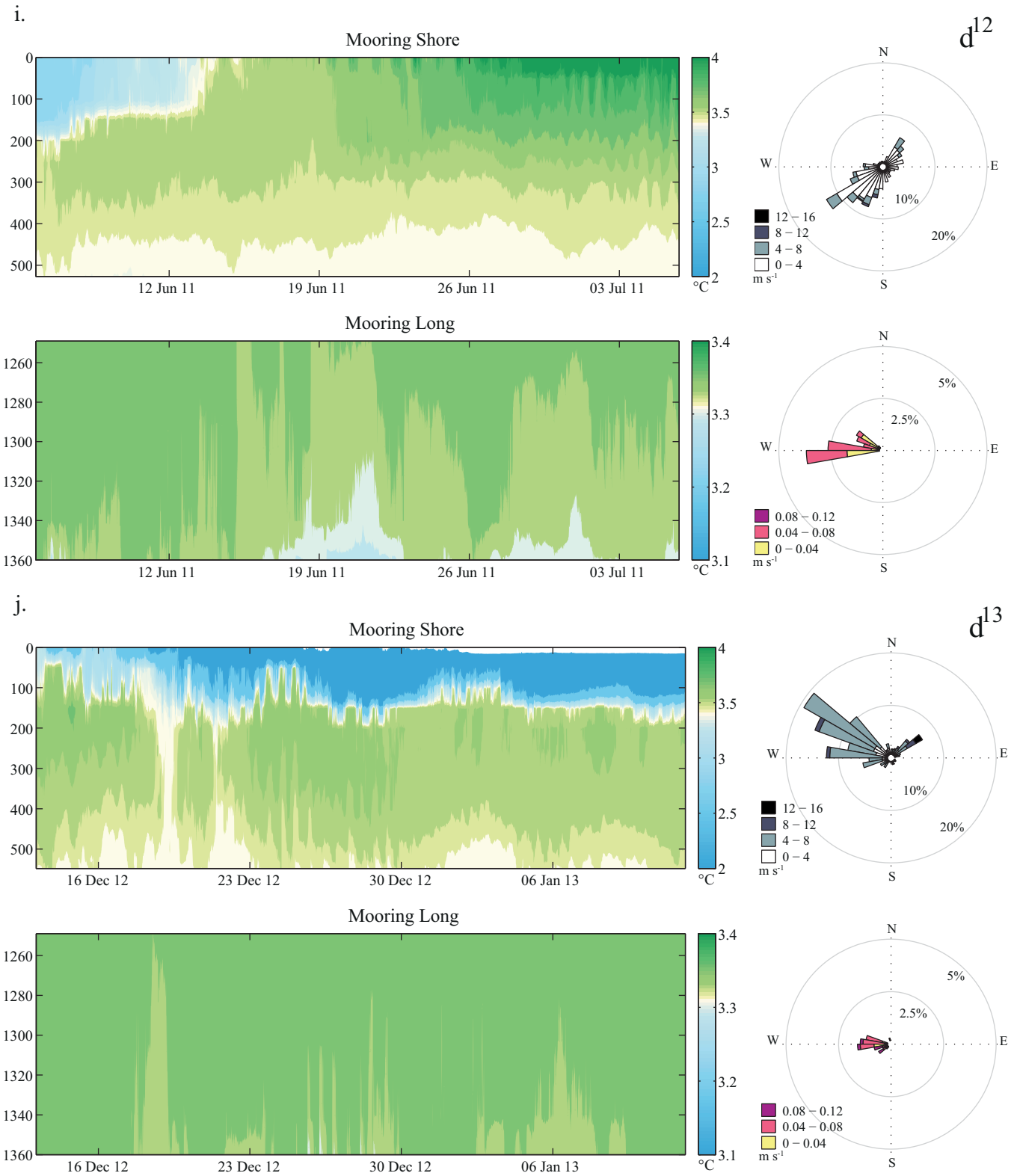

Figure 6. (continued)

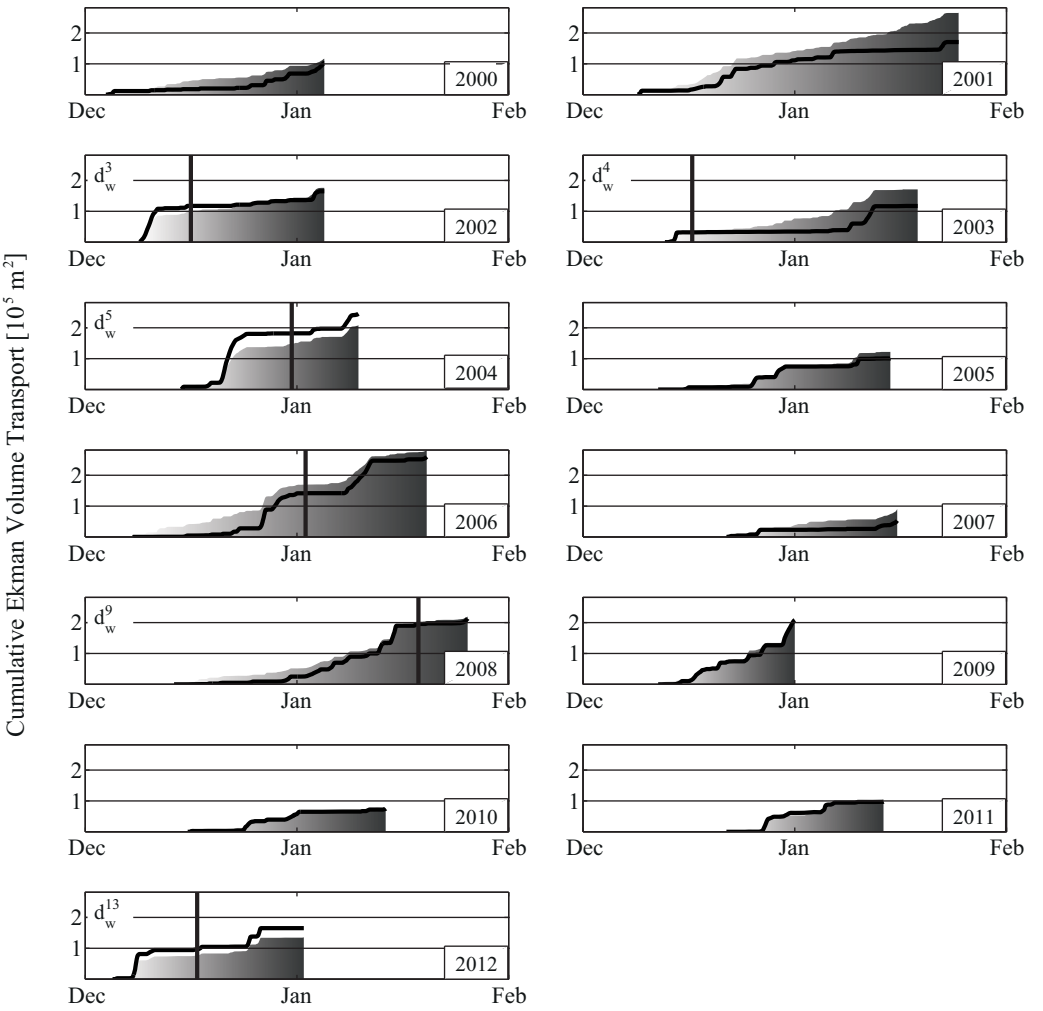

Figure 7. Cumulative Ekman transport calculated for the period allowing for downwelling before ice cover for each year from 2000 to 2012. The shaded area represents the average cumulative transport over the northern coast of the South Basin of Lake Baikal and the black line the cumulative transport at the monitoring station.

currents preceded the spring event d_s^8, while before the winter event d_w^9 no significant current activity was recorded. At 1350 m depth, currents were recorded for all events after 2007 with the exception of events d_s^8 and d_i^{10} when no activity was observed (the speed was probably lower than the threshold). The currents at the bottom for all the events are mainly alongshore in an anticlockwise direction with average speeds of 0.05 m s^{-1} and reaching a maximum of 0.12 m s^{-1}.

4.4. Events Not Explained by Observed Downwelling

The events not directly associated with downwelling, fall into two categories: the under-ice and the spring events. By default when the lake is ice covered, the wind cannot affect the water dynamics for downwelling to be triggered. In both cases, we can assume that either coastal downwelling happened at some other point along the northern coast of the South Basin (before the lake was ice covered) or that the deep-water renewal event was triggered by another mechanism. Under any scenario, the cold water mass would travel as a bottom current along the topography and/or spread by diffusion when it reached the bottom of the lake. From the six events of this category (d_i^5, d_i^{10}, and d_i^{11} under-ice and d_s^7, d_s^8, and d_s^{12} springtime), four had the cold-water front appearing first at mooring H and then at L. For d_i^{10} the main cold-water front had a 2 day lag between the two moorings, and for d_s^8, d_i^{11}, and d_s^{12} the lag was 16, 12, and 18 h, respectively. Taking under consideration that the distance between the two moorings is 1 km and that the threshold of the current meter is 0.02 m s^{-1}, the lag would have to be shorter than 14 h for the current to be detectable. This probably explains the fact that there were no current recordings for d_s^8 and d_i^{10}.

5. Discussion

5.1. Ekman Transport

The observations indicate that the driving mechanism of the winter events is coastal downwelling. Strong winds, which are prerequisite for downwelling, were observed during all winters; however, bottom-reaching cold intrusion events were not recorded each year. To have an insight, we calculated the Ekman transport resulting from the wind along the northern coast. It serves as a quantitative measure in order to correlate the temperature observations to the wind and stratification. Because the wind is highly variable and so is the wind stress, we look into the cumulative Ekman transport instead of the instantaneous values. The cumulative transport was calculated for each year from the day when the near-surface temperature at 16 m depth was approaching the bottom temperature until the lake was ice covered. We use the rotated coordinate system defined in paragraph 3.3 and calculated the transport component ($\vec{M}_q$) directed toward the coast at the area of the monitoring site and at the entire length of the northern coast of the South Basin. We found that the former is representative of the latter (Figure 7). For all winters, only when the transport toward the coast was sudden and intense a cold water mass appeared at the bottom of the lake. As the cumulative transport alone is not a measure of whether downwelling will occur, we calculated the rate at which it increased. We find that this rate of increase has to pass the threshold value of 2.5×10^3 m^2 (volume transport per unit meter of alongshore distance) per day in order for a bottom-reaching intrusion to be observed under these conditions. This allows us to differentiate between years with and without downwelling events by examining only the cumulative transport. It thus gives the possibility of event prediction considering solely the wind pattern at the monitoring area and information on lake surface temperature.

We found the Ekman transport component directed toward the southern coast to be two to three orders of magnitude stronger than that toward the northern coast during wintertime. This transport, however, does not result in downwelling. The southern slope is only $\sim 7.5^\circ$ steep, while the northern one is about $\sim 21.5^\circ$. An isotherm depression at the southern coast will therefore most probably result in a movement of the water mass along the bathymetry ruling out the Ekman downwelling scenario.

5.2. Spring Events

Contrary to the winter events, isotherm depression did not precede any of the observed spring events. Assuming that coastal downwelling cannot result in a deep intrusion at the south shore of the basin, we expect that the events were triggered by another mechanism. *Hohmann et al*. [1997] showed that colder and slightly more saline river water from the Selenga delta region can form sinking plumes in a short time slot between late April and May. The formation of the sinking plumes was identified mainly in the Central Basin and varied from year to year depending on the river outflow. *Wüest et al*. [2005] discarded this triggering mechanism for the South Basin because the ion or particle content of the cold near-bottom intrusions was not found significant. Due to lack of salinity and particle measurements in our data set, we cannot support deep-water formation at the Selenga delta region due to dense plume creation. However, we strongly suggest this to be the focus of a more thorough investigation.

5.3. Heat Content and Intruding Volume

We can get an indication of the downwelled water volume per event by calculating the heat content change in the deep-water. *Crawford and Collier* [1997] used a similar approach to calculate the volumes of deep mixing events in Crater Lake. The net heat change content in the lower bottom layer of the South Basin ($>$ 1250 m depth) is: $\Delta H = H(t_2) - H(t_1)$, where t_1 and t_2 correspond to the monthly averages of the month before and after the event accordingly. The heat content at t_1 and t_2 is calculated by:

$$H = \int_{z=1350\text{m}}^{z=1250\text{m}} \rho c_p T(z) A(z) dz \tag{5}$$

where ρ is the density, c_p the specific heat capacity at constant pressure, $T(z)$ the temperature, and $A(z)$ is the lake area, both a function of depth. By equating the heat change in the hypolimnion to the heat change introduced by the downwelled water mass, we approximate the volume, ΔV, by:

$$\Delta V = \frac{\Delta H}{\rho c_p (T_{down} - T_{back})} \quad (6)$$

where T_{down} is the minimum observed temperature of the cold water mass and T_{back} is the pre-event background temperature of the deep water at 1350 m depth. The intruding volumes vary between 27 and 200 km^3 per event, with an average of 83 km^3 (Table 1). Our results, although slightly larger, are comparable to the indirect annual steady state estimate of 30–70 km^3 yr^{-1} of intruding water to the PSDW (depth $>$ 300 m) by *Wüest et al*. [2005].

The estimation of the volume ΔV is sensitive to the temperature difference $T_{down} - T_{back}$. We assume that the minimum observed temperature T_{down} is representative of the intruding water mass. This assumption can lead to both an underestimation and an overestimation of the volume: an underestimation because water of a higher temperature is also transported and an overestimation because the event might not have taken place directly at the monitoring site. If this is the case, the real temperature could be even lower than the one observed. The volume for the event d_w^2 (171 km^3) is expected to be particularly overestimated. During the monitoring year 2002/2003 that d_w^2 took place, the temperature at 1350 m was used for the entire depth range (1250–1350 m) when calculating the heat change ΔH at the nominator of equation (5). This was done because no other thermistor was installed at this depth range that year.

The negative heat introduced by the near-surface water masses is eventually balanced by the vertical downward heat diffusion and the upward geothermal heat flux. Due to the high vertical diffusivity values of 10^{-4} to 10^{-3} m^2 s^{-1} in the PSDW and up to 10^{-2} m^2 s^{-1} in the bottom layer [*Wüest and Lorke*, 2003], the recovery to the background temperature of 3.35°C is relatively fast (less than 1 year as evident in Figure 5).

5.4. Summary

A total of 13 cooling events were observed when near-surface water reached the bottom of the South Basin at 1350 m depth. The occurrence of these events was evaluated in terms of the stratification, the currents, and the wind field. This evaluation showed that the events are occurring in three different periods each with distinct characteristics. (1) Six winter events followed Ekman coastal downwelling at the northern coast. The isotherm depression is taking place at the vicinity of our monitoring site just before completion of the ice cover of the lake. The stratification at this time period is optimal for deep vertical water displacements, allowing for thermobaric instability to occur that leads to deep dislocation of the initial isotherm depression caused by the wind. The observations over the monitoring site represented well the average Ekman transport over the north shore of the basin. (2) Three events were observed when the lake is ice covered. These events could have been triggered by coastal downwelling before the completion of the ice cover of the South Basin at an area further away from the monitoring site. However, we did not observe an increased Ekman transport during the preceding winters over the entire north coast. The causes of those events remain still unclear. (3) Four spring events were observed shortly after the ice breakup. These events do not show any correlation with the wind conditions over the South Basin and do not follow an isotherm depression. They are possibly connected to the increased spring outflow of cold and dense water of the Selenga River.

Convective episodic deep-water renewal is common in other deep lakes with a permanent stratification [*Boehrer and Schultze*, 2008]. The generation mechanism of the plunging water varies for each lake depending on the local topographic setting and the meteorological conditions. For example, in Lake Malawi cold intrusions most probably originate from dense, particle-loaded river plumes [*Vollmer et al*., 2005], while in Lake Issyk-Kul they are most likely generated by differential cooling in the shallow shelf [*Peeters et al*., 2003]. A lake whose physical mechanism resembles Lake Baikal is Crater Lake [*Crawford and Collier*, 1997, 2007]. However, this lake is small compared to Baikal. The same holds for a number of other relatively small but deep lakes in Japan and in Norway studied by *Boehrer et al*. [2008, 2013]. The common feature of these lakes to Baikal is the thermal stratification and the transition of epilimnion temperatures below 4°C in winter. They all have the potential of free convection of near-surface cold water masses; however, Ekman transport is ruled out as a triggering mechanism as their size is too small.

5.5. Outlook

Winter downwelling represents ~50% of the total observed cold-water bottom-reaching mass intrusions, with spring events holding ~30% and under-ice events ~20% of the total cold intrusion volumes. By calculating

the cumulative Ekman transport for the time period allowing for downwelling before the ice cover for all years, we were able to differentiate between the winters with and without downwelling events. We thus can foresee whether downwelling in the winter is taking place by analyzing the wind pattern over the lake.

To be able to have a better qualitative overview of the deep-water renewal events and their driving mechanisms, we would need to monitor closely the Selenga delta outflow region at the South Basin and combine precise current meter measurements with salinity and particle concentration measurements. Further, a network of reliable meteorological stations would be required to capture the high wind variability in space and time, facilitating a more accurate prediction tool.

Acknowledgments

This work was supported by the Scientific & Technological Cooperation Program Switzerland-Russia (IZLRZ2_128306), the Swiss National Science Foundation (grant 200020_144449), RFBR (grant 14–45-04053), and RSCF (grant 14-12-00128). A base part of Government Assignment for Scientific Research from the Ministry of Education and Science, Russia (N°2014/51, project 1366). The authors wish to thank: Michael Schurter, responsible for the data collection and instrument maintenance, for his yearlong fieldwork support on this project, Elena Vologina and Elena Troitskaya for their support in the field and their comments, KellyAnn Ross for her help in preparing the bathymetric map (Figure 1). The temperature and current meter data from the moorings and the wind output of the regional downscaling of the global NCEP-RA1 reanalysis product are available upon request from the corresponding author (chrysanthi.tsimitri@eawag.ch). The CTD data were provided by the Limnological Institute of the Siberian Branch of the Russian Academy of Science and are also available upon request from the corresponding author (chrysanthi.tsimitri@eawag.ch); the satellite images from the Moderate Resolution Imaging Spectroradiometer (MODIS) sensor of the Baikal area can be found on the website http://geol.irk.ru.

References

Akitomo, K., K. Tanaka, T. Awaji, and N. Imasato (1995), Deep convection in a lake triggered by wind: Two-dimensional numerical experiments with a nonhydrostatic model, *J. Oceanogr.*, *51*(2), 171–185, doi:10.1007/BF02236523.

Boehrer, B., and M. Schultze (2008), Stratification of lakes, *Rev. Geophys.*, *46*, RG2005, doi:10.1029/2006RG000210.

Boehrer, B., R. Fukuyama, and K. Chikita (2008), Stratification of very deep, thermally stratified lakes, *Geophys. Res. Lett.*, *35*, L16405, doi:10.1029/2008GL034519.

Boehrer, B., L. Golmen, J. E. Løvik, K. Rahn, and D. Klaveness (2013), Thermobaric stratification in very deep Norwegian freshwater lakes, *J. Great Lakes Res.*, *39*(4), 690–695, doi:10.1016/j.jglr.2013.08.003.

Botte, V., and A. Kay (2002), A model of the wind-driven circulation in Lake Baikal, *Dyn. Atmos. Ocean.*, *35*(2), 131–152, doi:10.1016/S0377-0265(01)00086-0.

Cotter, G. (2010), A Study of the change in the temperature of maximum density of water and aqueous solutions as a function of pressure, PhD thesis, Dep. of Exp. Physics, Nat. Univ. of Ireland, Maynooth, Co. Kildare, Ireland.

Crawford, G. B., and R. W. Collier (1997), Observations of a deep-mixing event in Crater Lake, Oregon, *Limnol. Oceanogr.*, *42*(2), 299–306.

Crawford, G. B., and R. W. Collier (2007), Long-term observations of deepwater renewal in Crater Lake, Oregon, *Hydrobiologia*, *574*, 47–68, doi:10.1007/s10750-006-0345-3.

De Batist, M., J. Klerkx, P. Van Rensbergen, M. Vanneste, J. Poort, A. Y. Golmshtok, A. A. Kremlev, O. M. Khlystov, and P. Krinitsky (2002), Active hydrate destabilization in Lake Baikal, Siberia?, *Terra Nova*, *14*(6), 436–442, doi:10.1046/j.1365–3121.2002.00449.x.

Dee, D. P., et al. (2011), The ERA-Interim reanalysis: Configuration and performance of the data assimilation system, *Q. J. R. Meteorol. Soc.*, *137*(656), 553–597, doi:10.1002/qj.828.

Delvaux, D., R. Moeys, G. Stapel, C. Petit, K. Levi, A. Miroshnichenko, V. Ruzhich, and V. San'kov (1997), Paleostress reconstructions and geodynamics of the Baikal region, Central Asia, Part 2. Cenozoic rifting, *Tectonophysics*, *282*(1-4), 1–38, doi:10.1016/S0040–1951(97)00210-2.

Hohmann, R., R. Kipfer, F. Peeters, G. Piepke, and D. M. Imboden (1997), Processes of deep-water renewal in Lake Baikal, *Limnol. Oceanogr.*, *42*(5), 841–855.

Kalnay, E. et al. (1996), The NCEP/NCAR 40-year reanalysis project, *Bull. Am. Meteorol. Soc.*, *77*(3), 437–471, doi:10.1175/1520-0477(1996)077<0437:TNYRP>2.0.CO;2.

Klehmet, K., B. Geyer, and B. Rockel (2013), A regional climate model hindcast for Siberia: Analysis of snow water equivalent, *Cryosphere*, *7*(4), 1017–1034, doi:10.5194/tc-7–1017-2013.

Kouraev, A. V., S. V. Semovski, M. N. Shimaraev, N. M. Mognard, B. Legrésy, and F. Rémy (2007), The ice regime of Lake Baikal from historical and satellite data: Relationship to air temperature, dynamical, and other factors, *Limnol. Oceanogr.*, *52*(3), 1268–1286, doi:10.4319/lo.2007.52.3.1268.

Lorke, A., and A. Wüest (2002), Probability density of displacement and overturning length scales under diverse stratification, *J. Geophys. Res.*, *107*(C12), 3214, doi:10.1029/2001JC001154.

Mackay, A. W. (2007), The paleoclimatology of Lake Baikal: A diatom synthesis and prospectus, *Earth Sci. Rev.*, *82*, 181–215, doi:10.1016/j.earscirev.2007.03.002.

Moore, M. V., S. E. Hampton, L. R. Izmest'eva, E. A. Silow, E. V. Peshkova, and B. K. Pavlov (2009), Climate change and the World's "Sacred Sea"—Lake Baikal, Siberia, *Bioscience*, *59*(5), 405–417, doi:10.1525/bio.2009.59.5.8.

Peeters, F., R. Kipfer, R. Hohmann, M. Hofer, D. M. Imboden, G. G. Kodenev, and T. Khozder (1997), Modeling transport rates in Lake Baikal: Gas exchange and deep water renewal, *Environ. Sci. Technol.*, *31*(10), 2973–2982, doi:10.1021/es9700459.

Peeters, F., D. Finger, M. Hofer, M. Brennwald, D. M. Livingstone, and R. Kipfer (2003), Deep-water renewal in Lake Issyk-Kul driven by differential cooling, *Limnol. Oceanogr.*, *48*(4), 1419–1431.

Piccolroaz, S., and M. Toffolon (2013), Deep water renewal in Lake Baikal: A model for long-term analyses, *J. Geophys. Res. Oceans*, *118*, 6717–6733, doi:10.1002/2013JC009029.

Ravens, T., O. Kocsis, A. Wüest, and N. Granin (2000), Small-scale turbulence and vertical mixing in Lake Baikal, *Limnol. Oceanogr.*, *45*(1), 159–173, doi:10.4319/lo.2000.45.1.0159.

Rockel, B., A. Will, and A. Hense (2008), The Regional Climate Model COSMO-CLM (CCLM), *Meteorol. Z.*, *17*(4), 347–348, doi:10.1127/0941–2948/2008/0309.

Sapota, T., L. Håkanson, A. Aldahan, and G. Possnert (2006), Sediment flux to Lake Baikal (Siberia, Russia): Modeling approach, *Geomorphology*, *80*(1-2), 105–113, doi:10.1016/j.geomorph.2005.09.009.

Schmid, M., N. M. Budnev, N. G. Granin, M. Sturm, M. Schurter, and A. Wüest (2008), Lake Baikal deepwater renewal mystery solved, *Geophys. Res. Lett.*, *35*, L09605, doi:10.1029/2008GL033223.

Shimaraev, M. N., N. G. Granin, and A. A. Zhdanov (1993), Deep ventilation of Lake Baikal waters due to spring thermal bars, *Limnol. Oceanogr.*, *38*(5), 1068–1072, doi:10.4319/lo.1993.38.5.1068.

Shimaraev, M. N., V. I. Verbolov, N. G. Granin, and P. P. Sherstyankin (1994), *Physical Limnology of Lake Baikal: A Review*, Baikal Int. Cent. of Ecol. Res., Irkutsk.

Smith, S. D. (1988), Coefficients for sea surface wind stress, heat flux, and wind profiles as a function of wind speed and temperature, *J. Geophys. Res.*, *93*(C12), 15,467–15,472, doi:10.1029/JC093iC12p15467.

Steppeler, J., G. Doms, U. Schättler, H. W. Bitzer, A. Gassmann, U. Damrath, and G. Gregoric (2003), Meso-gamma scale forecasts using the nonhydrostatic model LM, *Meteorol. Atmos. Phys.*, *82*(1-4), 75–96, doi:10.1007/s00703-001-0592-9.

Troitskaya, E., V. Blinov, V. Ivanov, A. Zhdanov, R. Gnatovsky, E. Sutyrina, and M. Shimaraev (2015), Cyclonic circulation and upwelling in Lake Baikal, *Aquat. Sci.*, *77*(2), doi:10.1007/s00027-014-0361-8, in press.

Vollmer, M. K., H. A. Bootsma, R. E. Hecky, G. Patterson, J. D. Halfman, J. M. Edmond, D. H. Eccles, and R. F. Weiss (2005), Deep-water warming trend in Lake Malawi, East Africa, *Limnol. Oceanogr.*, *50*(2), 727–732, doi:10.4319/lo.2005.50.2.0727.

Weiss, R. F., E. C. Carmack, and V. M. Koropalov (1991), Deep-water renewal and biological production in Lake Baikal, *Nature*, *349*(6311), 665–669, doi:10.1038/349665a0.

Wüest, A., and A. Lorke (2003), Small-scale hydrodynamics in lakes, *Annu. Rev. Fluid Mech.*, *35*, 373–412, doi:10.1146/annurev.fluid.35.101101.161220.

Wüest, A., T. Ravens, N. Granin, O. Kocsis, M. Schurter, and M. Sturm (2005), Cold intrusions in Lake Baikal: Direct observational evidence for deep-water renewal, *Limnol. Oceanogr.*, *50*(1), 184–196, doi:10.4319/lo.2005.50.1.0184.

Yelland, M., and P. K. Taylor (1996), Wind stress measurements from the open ocean, *J. Phys. Oceanogr.*, *26*(4), 541–558, doi:10.1175/1520-0485(1996)026<0541:WSMFTO>2.0.CO;2.

Erratum

In the originally published version of this article, in Figure 6, parts i and j were missing from the PDF. This error has since been corrected and this version may be considered the authoritative version of record.